Eur. Phys. J. B **21**, 93–102 (2001)

THE EUROPEAN PHYSICAL JOURNAL B

EDP Sciences

Topological and dynamical excitations in a classical 2D easy-axis Heisenberg model

T. Kamppeter[1], S.A. Leonel[2], F.G. Mertens[1], M.E. Gouvêa[3,a], A.S.T. Pires[3], and A.S. Kovalev[4]

[1] Physikalisches Institut, Universität Bayreuth, 95440 Bayreuth, Germany
[2] Departamento de Física, ICE, Universidade Federal de Juiz de Fora, Juiz de Fora, CEP 36036-330, MG, Brazil
[3] Departamento de Física, ICEx, Universidade Federal de Minas Gerais, Belo Horizonte, CP 702, CEP 30123-970, MG, Brazil
[4] Institute for Low Temperature Physics and Engineering, 310164, Kharkov, Ukraine

Received 22 August 2000

Abstract. The properties of dynamical solitons (magnon droplets) in the classical, two-dimensional anisotropic Heisenberg model with easy-axis exchange anisotropy are studied. The solution of the Landau-Lifshitz equation in the continuum limit for the soliton with topological charge $q = 1$ is obtained numerically using a shooting method. We analized a wide range of the anisotropy parameter and our results are in good agreement with results obtained from spin dynamics simulations. The dependence of an internal precession frequency of the soliton on both the anisotropy parameter and the radius of the soliton is also investigated. Finally, the limits of applicability of the continuum approach are discussed.

PACS. 75.10.Hk Classical spin models – 75.30.Et Exchange and superexchange interactions – 75.70.Kw Domain structure (including magnetic bubbles)

1 Introduction

Linear (spin waves) and nonlinear (domain walls) dynamical excitations of magnetically ordered media have represented the traditional objects of experimental and theoretical study for many years. Particularly, the nonlinear dynamics of magnets was investigated intensively during the last three decades in the general context of "nonlinear science" [1,2]. Several types of dynamical and topological magnetic solitons were studied theoretically and their existence was confirmed experimentally. Most of the main theoretical results were obtained in the long-wave approximation, in the framework of simple (usually one-dimensional and often integrable) models which describe the classical Heisenberg magnets with small single-ion magnetic anisotropy. However, in the last few years, many new low-dimensional magnetic compounds with unique properties were synthesized producing a radical change in the problems to be studied [3]. Examples of such materials include most of the undoped high-temperature superconductors and their isostructural analogues which have a layered antiferromagnetic structure, quasi-one-dimensional magnets $[(CH_3)_3NH]NiCl_3 2H_2O$, $(C_9H_7NH)NiCl_3 1.5H_2O$ [4], layered intercalated easy-axis antiferromagnets as $(CH_2)_n(NH_3)_2MnCl_4$, and $(C_nH_{2n+1}NH_3)_2MnCl_4$ [5–8], the metalorganic layered easy-plane antiferromagnets $(NH_3)_2(CH_2)_nCuCl_4$ [9] and the layered metalorganic ferromagnet $(CH_3NH_3)_2CuCl_4$ (MACC) [3,10]. In these compounds, it is possible to change the number n of organic molecules intercalating the magnetic layers which opens the possibility of experimental investigation of the dependence of the structure and of dynamic properties of such magnets on the value of the exchange integral (in comparison with the anisotropy). Experiments performed on these materials showed the existence of strong and unusual nonlinear effects such as chaotic behavior [10] and power adsorption in the gap of the spin waves spectrum [11]. These results can not be explained in the framework of the usual theoretical models due to the essential discreteness of the mentioned materials. On the other hand, low-dimensional magnets may, in some cases, exhibit a considerable anisotropy of the exchange interaction, while most theoretical models take into account only single-ion or weak exchange anisotropy. The actual anisotropy of exchange can be of order of the exchange interaction itself. For example, the g-factor anisotropy in the compounds $KDy(MoO_4)_2$ and $KEr(MoO_4)_2$ is of order of 20 [12]. The study of cases like the ones cited above requires a recast of most of the available theoretical results.

For one-dimensional magnetic chains with strong single-ion and exchange anisotropies some results were obtained in [13–15]. In the two-dimensional case the theoretical situation is much more complicated and the use of numerical simulations is necessary, especially for the description of 2D dynamical and topological solitons and vortices in layered magnets with strong magnetic

[a] e-mail: meg@aquila.fisica.ufmg.br

anisotropy. Most of the existing results for 2D solitons and vortices concerned ferromagnets with small single-ion anisotropy [1,2,8,16–18], although some results [19,20] were also obtained for ferromagnets with small exchange anisotropy. In these two cases, the structure and dynamics of 2D vortices and solitons are very similar. However, for strong anisotropy, the results for single-ion and exchange anisotropy must be different and, more importantly, may differ appreciably from the small anisotropy regime.

In this paper we are interested in the properties of two-dimensional localized topological solitons (sometimes named vortices due to their in-plane spin structure) in the classical ferromagnetic Heisenberg model with easy-axis exchange anisotropy in a wide region of values for the anisotropy parameter. The interest devoted to solitons in easy-axis magnetic systems was considerably smaller than that to vortices in easy-plane materials because, in the latter case, the presence of vortex-antivortex pairs, and their unbinding, is directly related to the Kosterlitz-Thouless phase transition. Nevertheless, topological excitations in easy-axis ferromagnets attract theoretical interest due to their special dynamics: soliton mobility connected with its finite mass, the existence of internal modes in the soliton, and the possibility of loss of topological properties in the strong anisotropy limit. Recently the novel interest to such objects (often named "skyrmions") is connected with the observation of the skyrmions in 2D electron layers under the quantum Hall effect conditions.

It is important to remark that vortices in easy-axis magnets were observed experimentally in the experiments performed by Waldner [7,8,21]. Although the experimental data obtained by Waldner for the energy of 2D magnetic excitations are in excellent agreement with the theoretical predictions, some questions were not completely clarified and remain open until now. First of all the experiments have been pursued with layered antiferromagnets while the minimum energy was calculated for the static ferromagnetic vortex. However, it follows from simple theoretical models that the minimum of energy in 2D ferromagnets corresponds to the energy of the dynamical singular vortex with the frequency of a homogeneous ferromagnetic resonance [1,16,18]; this value is very close to the energy of 2D nontopological dynamical solitons [16]. Moreover, in general, vortices do not exist in the same model for 2D antiferromagnets [22]. Later it was predicted theoretically [23,24] that the static ferromagnetic vortex can exist if the discreteness of the lattice is taken into account. However, this prediction leads to a static vortex radius far less than the interatomic distance. These fact indicate that new analytical and numerical investigations of the skyrmions-type magnetic vortices are a necessity. Numerical simulations are particularly important to understand the effects of discreteness.

We investigate the structure of the soliton with topological charge $q = 1$ in the continuum limit and, also, in the discrete system by using spin dynamics simulations. The equation of motion in the continuum limit leads to an ordinary differential equation (ODE) for the radial structure of the excitation which cannot be analytically solved but we were able to find its asymptotic analytical solutions, and, then, to gain some insight about the shape of the structure. These asymptotic solutions are used as a starting point in the procedure adopted for the numerical solution of the ODE. The results thus obtained, as well as the ones obtained from the spin dynamics simulations, are in good agreement for a wide range of the anisotropy parameter. The dependences of the internal precession frequency on the magnetic anisotropy and on the soliton radius (the number of magnons bound in the soliton) are also given.

2 Model

We start by considering the classical two-dimensional ferromagnetic Heisenberg model with uni-axial magnetic anisotropy of two different types

$$\mathcal{H} = -J \sum_{n,m} \left[S_x^n S_x^m + S_y^n S_y^m + (1+K) S_z^n S_z^m \right] - dJ \sum_n (S_z^n)^2 \tag{1}$$

where the summations run over all nearest-neighbor sites n and m of the classical spin vectors $\mathbf{S}^n$. Here, J denotes the exchange integral ($J > 0$ for ferromagnets), the parameter K denotes the exchange interaction anisotropy and d characterizes the single-ion (on site) anisotropy. We will consider only the so-called Ising-type ferromagnets with $K > 0$ and $d > 0$ supposing that these two anisotropies have the same symmetry with respect to the z-direction.

The classical dynamics of a spin system without damping can be described by the Landau-Lifshitz equation

$$\hbar \frac{\mathrm{d}\mathbf{S}^n}{\mathrm{d}t} = -\mathbf{S}^n \times \frac{\partial \mathcal{H}}{\partial \mathbf{S}^n} \cdot \tag{2}$$

It is convenient to measure the time in units of $JS_0/\hbar$ where S_0 is the length of the spins. Then, we can rewrite equation (2) in terms of the unit vectors $\mathbf{s}^n$ as

$$\frac{\mathrm{d}\mathbf{s}^n}{\mathrm{d}t} = \sum_m (\mathbf{s}^n \times \mathbf{s}^m) + K\,(\mathbf{s}^n \times \mathbf{e}_z) \sum_m s_z^m + 2\,d\,(\mathbf{s}^n \times \mathbf{e}_z)\, s_z^n \cdot \tag{3}$$

The dispersion relation of spin waves of the form $s_x^n + \mathrm{i} s_y^n \sim \exp\bigl(\mathrm{i}(kn - \omega t)\bigr)$ on the discrete lattice is

$$\omega(q) = \omega_0 + 4\ \sin^2 \frac{q}{2} \tag{4}$$

where $\omega_0 = 2(2K + d)$ is known as the homogeneous ferromagnetic resonance frequency.

In the long-wave approximation, valid for small anisotropy values ($K, d \ll 1$), equation (3) becomes

$$\frac{\mathrm{d}\mathbf{s}}{\mathrm{d}t} = \mathbf{s} \times \Delta\mathbf{s} + 2(2K + d)\,(\mathbf{s} \times \mathbf{e}_z)\, s_z, \tag{5}$$

where we have set the interatomic distance $a = 1$. Notice that, as in equation (5), the two types of anisotropy appear combined as $2(2K+d) = 4\tilde{K}$. This combination characterizes the time and space scales of the magnetic excitations: the frequency ω_0 defined before, and the so-called "magnetic length", $l_0 = 1/\sqrt{4\tilde{K}}$. In the case of weak anisotropy, the gap in the spin wave spectrum ($0 < \omega < \omega_0$) is narrow in comparison to the width of the spectrum band ($\sim$1 in our units), and the magnetic length is much larger than the interatomic distance.

However, in the discrete limit (so-called "anti-integrable limit") when the magnetic anisotropy is of the order of the exchange interaction (*i.e.* the parameters K and d are of order of unity), the influence of each kind of anisotropy on the properties of *nonlinear* excitations may be different. We achieve this conclusion by considering the structure of a domain wall on a spin chain. The width of the wall is characterized by the magnetic length l_0 and decreases as the anisotropy increases. For the one-dimensional case (1D), it was shown [25] that only when the existing anisotropy is of the single-ion type the domain wall can transform itself into a collinear structure. In the case of pure exchange anisotropy it conserves its canted form for any value of the anisotropy parameter K. This problem is important for us because the solitons in the 2D lattice that will be studied here have the form of a cylindrical domain wall in the limit of a large number of magnons bound in the soliton.

In order to recover the main results obtained for the 1D case, we will summarize here the main steps of the treatment used in [25]. It is convenient to introduce the complex variables $\psi^n = s_x^n + \mathrm{i}s_y^n$ and rewrite the equation of motion (3) in the one-dimensional case in the form

$$\mathrm{i}\frac{\mathrm{d}\psi^n}{\mathrm{d}t} = (1+K)\ \psi^n\ (s_z^{n+1} + s_z^{n-1}) - s_z^n\ (\psi^{n+1} + \psi^{n-1})\ +\ 2ds_z^n\psi^n. \quad (6)$$

The collinear form of the domain wall corresponds to the following spin configuration: $s_z^n = -1$ for $n \geq 1$ and $s_z^n = 1$ for $n \leq 0$. After linearizing equation (6) with respect to small deviations of ψ_n from this configuration, we obtain for the frequency of the solution localized near the domain wall ("internal mode") the following relation

$$\left(\sqrt{(\omega/2 - K - d - 1)^2 - 1} - (\omega/2 + K - d + 1)\right) \times \left(\sqrt{(\omega/2 + K + d + 1)^2 - 1} - (-\omega/2 + K - d + 1)\right) = 1. \quad (7)$$

The frequency of the domain wall localized mode does not depend on the anisotropy parameters, K and d, in an obvious way. The stability of the collinear structure of the domain wall requires the frequency ω to be real, and thus the line $\omega = 0$ on the (K, d)-plane corresponds to the boundary of existence of collinear domain walls. This line is defined by

$$d_\mathrm{c} = \frac{2 + K_\mathrm{c}}{3 + 2K_\mathrm{c}}\,. \quad (8)$$

The region $d > d_\mathrm{c}$ on this plane corresponds to collinear domain walls. The domain wall has a canted form for any value of the exchange anisotropy K if the on-site anisotropy is smaller than 1/2. (The transformation of collinear domain walls into the canted form in the simplest case of $K = 0$ was investigated in [13,26,27]).

In the case of a pure exchange anisotropy in a ferromagnet, the domain wall has a canted form for all values of K and an exact solution for it is well known [28]

$$\psi^n = \frac{1}{\cosh(\nu n + \nu_0)}, \quad (9)$$

where $\cosh\nu = 1 + K$ in our notations and ν_0 is an arbitrary constant. The energy of the unit length of the domain wall is $E_0 = 2\sqrt{4K(1+K)}/(1+2K)$.

The *dynamical* properties of domain walls in ferromagnets with single-ion or exchange anisotropy are different, too: in the case of pure exchange anisotropy ($d = 0$) the Peierls relief for the solution (9) equals zero and the corresponding internal mode of the domain wall is absent, in contrast to the situation in magnets with on-site anisotropy only ($K = 0$).

Because of these results for 1D spin lattices, we expect similar qualitative differences for the solitons on 2D lattices with different kinds of anisotropies.

3 Integrals of motion

The pure on-site anisotropy ($K = 0$) was investigated in previous papers [1,29,30]. Here, we investigate the more general Hamiltonian (1) but, later, we will concentrate on the case of pure exchange interaction anisotropy ($d = 0$).

We will use below both the spherical coordinates for the spins

$$\mathbf{s}^n = (\sin\theta_n\cos\phi_n, \sin\theta_n\sin\phi_n, \cos\theta_n), \quad (10)$$

and the canonically conjugated coordinates, namely the in-plane angles ϕ_n and the out-of-plane components $m_n = s_z^n$, which gives

$$\mathbf{s}^n = (\sqrt{1-(m_n)^2}\ \cos\phi_n,\ \sqrt{1-(m_n)^2}\ \sin\phi_n, m_n). \quad (11)$$

In the Hamiltonian formalism, the equations of motion (6) in terms of the canonical coordinates have the form

$$\frac{\mathrm{d}m_n}{\mathrm{d}t} = \frac{\partial\mathcal{H}}{\partial\phi_n}, \quad (12a)$$

$$\frac{\mathrm{d}\phi_n}{\mathrm{d}t} = -\frac{\partial\mathcal{H}}{\partial m_n}, \quad (12b)$$

with the Hamiltonian given by

$$\mathcal{H} = -\sum_{n,m}\sqrt{1-m_n^2}\ \sqrt{1-m_m^2}\ \cos(\phi_n - \phi_m) - (1+K)\sum_{n,m} m_n m_m - d\sum_n m_n^2. \quad (13)$$

It follows from the first equation of motion (12a) that

$$\frac{\mathrm{d}}{\mathrm{d}t}\sum_n m_n = \sum_{n,m}\sqrt{1-m_n^2}\,\sqrt{1-m_m^2}\,\sin(\phi_n-\phi_n) = 0$$

which leads us to an integral of motion defined by

$$N = \sum_n (1-m_n) \tag{14}$$

for ferromagnets with all types of uni-axial magnetic anisotropies. This integral plays an important role in spin dynamics because it defines the number of magnons or spin deviations. Using the Lagrangian approach, it is easy to show (see, for example, [29]) that, for the one-frequency solutions, the quantity N coincides with the adiabatic invariant I of the system ($N = I/\hbar$) and gives the number of elementary excitations of the system under semiclassical quantization.

We will study below the magnetic solitons in easy-axis ferromagnets, which are stabilized by an additional precession of the magnetization with the angle $\phi_n = \omega t$. For such solutions, one can demonstrate that

$$\omega = \mathrm{d}\mathcal{H}/\mathrm{d}N \tag{15}$$

by varying the integrals of motion $\mathcal{H}$ and N. The frequency ω represents the chemical potential for the magnons in the system.

The above results also hold for systems with strong anisotropies where discreteness effects are important.

In the case of a 2D magnetic soliton, a third integral of motion needs to be considered; it is the topological charge, or vorticity. The expression for this topological charge in the continuum approximation is

$$q = \frac{1}{4\pi}\int \gamma\,\mathrm{d}x\mathrm{d}y, \tag{16}$$

where the quantity

$$\gamma = \Big(\frac{\partial m}{\partial x}\frac{\partial \phi}{\partial y} - \frac{\partial m}{\partial y}\frac{\partial \phi}{\partial x}\Big), \tag{17}$$

represents the so-called "vorticity density" [31,32]. On this reason the excitation can also be called vortex. For fixed boundary conditions, $m(r \to \infty) = 1$, the topological charge is equal to $q = \pm 1, \pm 2, ...$ and its sign depends on the direction of the rotation of the azimuthal angle ϕ along an arbitrary contour around the soliton center. (Note that, in easy-axis ferromagnets, the value $m(\infty) - m(0) = 2$ for the magnetic soliton is twice as large as in the easy-plane systems, moreover the definition of the topological charge differs from that in easy-plane magnets [20]).

4 Shape of the soliton

Now, we look for the soliton shape in the continuum limit which means that we will be restricted to small values for both the exchange and on-site anisotropies. We consider a single soliton in the center of a system much larger than the soliton size which is considered to be of at least some lattice constants ($K, d \ll 1$). Therefore we replace $\mathbf{S}^n(t)$ in (2) by the spin field $\mathbf{S}(\mathbf{r}, t)$. The Hamiltonian (1) in the variables ($\phi,\ m$) can be written as [12]:

$$\mathcal{H} = \frac{JS_0^2}{2}\int \mathrm{d}^2x\Big[\Big(1+K(1-m^2)\Big)\frac{(\nabla m)^2}{(1-m^2)} + (1-m^2)(\nabla\phi)^2 - 4\tilde{K}m^2\Big] \tag{18}$$

and the equations of motion in terms of ϕ and m have the form

$$\frac{\partial\phi}{\partial t} = \Big[-\frac{m}{(1-m^2)^2}(\nabla m)^2 - m(\nabla m)^2 - \frac{\Delta m}{1-m^2}\Big] - 4\tilde{K}m - K\Delta m, \tag{19a}$$

$$\frac{\partial m}{\partial t} = (1-m^2)\,\Delta\phi - 2\,m\,\nabla m\nabla\phi. \tag{19b}$$

The time is measured in units of $JS_0/\hbar$ as before.

In topological solitons, the magnetization m varies in the interval $[1,-1]$ and the azimuthal angle ϕ changes from 0 to $2\pi q$. Then the characteristic scales of the terms in equation (19a) are of the order of ∇^2 for the terms inside the brackets and $\tilde{K}$, and $K\nabla^2$, for the last two terms. Usually the size of the spatial inhomogeneity of the magnetization field is of the order of the magnetic length $l_0 = 1/2\sqrt{\tilde{K}}$ and since we are working in the continuum approximation we must have $l_0 \gg 1 (\tilde{K} \ll 1)$. In this case, $\nabla \sim 1/l_0 \sim \sqrt{\tilde{K}}$, and the first terms in (19a) are of the same order ($\sim \tilde{K}$), but the last term is much smaller ($\sim K^2$). This means that, in a self-consistent approach, one should take into account the additional dispersion terms proportional to $\nabla^4 \sim K^2$ in (19) — which would require the inclusion of higher order terms in Hamiltonian (18). However, this makes sense only for small anisotropies and our task here is to consider large ones too. Therefore, we restrict ourselves to the Hamiltonian (18), noting that the discreteness of the system is taken into account by the last term on the r.h.s.

The scheme adopted is self-consistent for large exchange and large single-ion anisotropy ($K \sim 1, d \sim 1$) if $d < 0$ and $2K \simeq |d|$ ($\tilde{K} \ll 1$). This situation was discussed in [15] where it was shown that in the limit $\tilde{K} \ll 1$, magnetic solitons and domain walls transform into an exotic compact form. Thus, in the 2D case, the soliton represents a cylindrical domain bounded by a circular domain wall of a radius R with profile $m = \sin\Big(2\sqrt{\tilde{K}/K}(r-R)\Big)$ and with magnetization $m = \pm 1$ outside the wall and ∓ 1 inside of it.

A precessing topological soliton does not translate and its center stays at the center of the circular system. It has axial symmetry and in polar coordinates (r, χ) it has the form

$$m = m(r), \qquad \phi = \omega t + q\chi, \tag{20}$$

where q is the topological charge (16) of the soliton, and ω is the precession frequency of all spins. Inserting (20) into equation (19a) we obtain an ordinary differential equation for $m(r)$:

$$\left(\frac{1}{1-m^2}+K\right)\left(\frac{\mathrm{d}^2m}{\mathrm{d}r^2}+\frac{1}{r}\frac{\mathrm{d}m}{\mathrm{d}r}\right)+\frac{m}{(1-m^2)^2}\left(\frac{\mathrm{d}m}{\mathrm{d}r}\right)^2 + m\left(4\tilde{K}+\frac{q^2}{r^2}\right)+\omega=0, \quad (21)$$

which, rewritten in terms of the spherical variable $\theta(r)$ defined in (10), becomes

$$-(K\sin^2\theta+1)\left(\frac{\mathrm{d}^2\theta}{\mathrm{d}r^2}+\frac{1}{r}\frac{\mathrm{d}\theta}{\mathrm{d}r}\right)-K\sin\theta\cos\theta\left(\frac{\mathrm{d}\theta}{\mathrm{d}r}\right)^2 + \sin\theta\cos\theta\left(4\tilde{K}+\frac{q^2}{r^2}\right)+\sin\theta\,\omega=0. \quad (22)$$

This equation was studied numerically in [16] for the particular case $K=0$, $\tilde{K}=2d$ (see also [1,29]).

Considering that in the ground state of an easy-axis ferromagnet all spins point either up ($\theta=0$) or down ($\theta=\pi$), we choose the following boundary conditions

$$\theta(r=0)=\pi, \quad (23a)$$
$$\theta(r=\infty)=0. \quad (23b)$$

(In the numerical simulations to be discussed in the next section, we will adopt fixed boundary conditions with all the spins at the border pointing up: $\theta(x=\pm L, y=\pm L)=0$). The same procedure was applied to a ferromagnet with pure single-ion anisotropy leading to an equation similar to (22) which, for that case, was solved numerically in [16]. In the next section, we will also solve numerically equation (22) but for systems with pure exchange anisotropy and then discuss the soliton soliton obtained. However, it is interesting to investigate analytically the asymptotic behavior of the soliton solution, and, later, compare it to the numerical results.

After linearizing (22) we obtain for the region around the center of the soliton ($r\to 0$), the modified Bessel equation

$$\rho^2\frac{\mathrm{d}^2\alpha}{\mathrm{d}\rho^2}+\rho\frac{\mathrm{d}\alpha}{\mathrm{d}\rho}-\left(\rho^2+q^2\right)\alpha=0, \quad (24)$$

where $\alpha=\pi-\theta$ is small angle in this region, and

$$\rho=\sqrt{\omega_0-\omega}\,r. \quad (25)$$

A nonsingular soliton solution with topological charge $q=1$ for (24) is given by $\alpha(\rho)=\alpha_0 I_1(\rho)$, and for the $r\to 0$ asymptotic behavior of θ we obtain

$$\theta(r)\simeq\pi-\frac{r}{r_0}, \quad (26)$$

where r_0 is an arbitrary constant.

The linearization of (22) with respect to the small angle θ, at large distances from the soliton center ($r\to\infty$), also gives us a modified Bessel equation

$$\zeta^2\frac{\mathrm{d}^2\theta}{\mathrm{d}\zeta^2}+\zeta\frac{\mathrm{d}\theta}{\mathrm{d}\zeta}-\left(\zeta^2+q^2\right)\theta=0 \quad (27)$$

where

$$\zeta=\sqrt{\omega_0+\omega}\,r \quad =r/r_\star. \quad (28)$$

Thus, the soliton solution with $q=1$ has the asymptotic form $\theta(r)\simeq\theta_0 K_1(\zeta)$ and decays exponentially as $r\to\infty$

$$\theta(r)\;\simeq\;\sqrt{\frac{r_\star}{r}}\mathrm{e}^{-r/r_\star}. \quad (29)$$

The constants r_0 and $r_\star$ in (26) and (29) depend on the frequency ω and can be determined by matching the asymptotic solutions (26) and (29) at intermediate distances.

The shape of a soliton depends essentially on the relation between the value of anisotropy constant $\tilde{K}$ and the number of magnons bound in soliton N (or its radius R). If the radius of a soliton is much larger than the magnetic length $R\gg l_0=1/\sqrt{4\tilde{K}}$, *i.e.* $N\gg 1/\tilde{K}$, a cylindrical domain wall is formed and the case corresponds to small precession frequencies $\omega\ll\omega_0$. In this limit we can use the solution for one-dimensional domain wall in the vicinity of the cylindrical wall bounding the soliton

$$\theta\;\simeq\;\pi\;-\;2\;\arctan\exp\left(\frac{r-R}{l_0}\right). \quad (30)$$

(This corresponds to the simplest form of 1D domain wall in ferromagnet with $K\ll d$. The solution for the case $K\sim d$ was obtained in [18]). The number of magnons bound in the soliton is proportional to its volume $N\simeq 2\pi R^2$ and the energy of the soliton is approximately equal to the energy of the cylindrical domain wall: $E\;\simeq\;2\pi RE_0\;=\;2\pi R\;2JS_0^2/l_0=8\pi R\sqrt{\tilde{K}}$. Using relation (25) we obtain the dependences of the soliton frequency ω (in units of $JS_0/\hbar$) on its radius R and on the anisotropy constant $\tilde{K}$

$$\omega\simeq\frac{1}{l_0R}=\frac{\sqrt{4\tilde{K}}}{R}\quad\text{or}\quad\frac{\omega}{\omega_0}\simeq\frac{l_0}{R}. \quad (31)$$

The inverse proportionality between ω and R could be expected since the mass of the soliton must increase with the soliton radius R; this relationship is confirmed by our numerical simulation results, as will be discussed in Section 5. Our numerical data also confirm the $\omega\propto\sqrt{\tilde{K}}$ relation.

In the opposite case of a soliton with small radius $R\ll l_0$ and high frequency $\omega\simeq\omega_0$, the profile of the θ-field in the center of a soliton has a sharp form. (Note that for small values of anisotropy the above inequalities are valid for large radii $R\gg 1$). In this limit an approximate expression for a soliton solution was proposed in [23] giving

$$\tan\left(\frac{\theta}{2}\right)\simeq\frac{2}{(q-1)!}\left(\frac{R}{2l}\right)^q K_q\left(\frac{r}{l}\right), \quad (32)$$

where q is the topological charge of the soliton and $l = l_0/\sqrt{1-\omega/\omega_0}$. For $q = 1$, we obtain

$$\omega \simeq 4\tilde{K}\left(1 + \frac{1}{\ln\left(R^2\tilde{K}\right)}\right), \tag{33}$$

which is the relation obtained in [23] and which plays the same role as (31) in this limit.

5 Spin dynamics simulations

The analytical and numerical analysis we have done so far is restricted to the continuum approximation and axial symmetrical form of a soliton. In the discrete limit of a ferromagnet with strong anisotropy, the width of a domain wall boundering the soliton is of order of the interatomic parameter and the wall has nearly collinear structure. In this limit, the long wave approximation and the investigation of soliton dynamics in the framework of differential equations for the magnetization are not valid. Moreover, in the the discrete limit the shape of the domain wall depends on its orientation with respect to the orientation of the lattice and the soliton – strictly speaking – does not have radial symmetry. This symmetrical geometry is broken even in long wave approximation if the system holding the vortex is not circular (as in our simulations where we chose a square system) and is not large enough in comparison to the soliton size. In all the cases above, we can not use equation (22) for the analytical and numerical investigations of a soliton.

In order to investigate discreteness effects on the soliton to be formed in easy-axis systems with pure exchange anisotropy, we will use spin dynamic simulations to study the model described by (1) with $d = 0$. In these simulations we will not be restricted neither to the discreteness of the solution nor to its radial symmetrical form or to boundary conditions. However, the following problems will appear in such approach. As we do not know the real solution, we will have to insert an approximate expression describing the vortex at the initial step of the simulation. The approximate form we will use has axial symmetry, radius R and width l_0' for the boundaring wall. Obviously, the soliton obtained as a result of the simulation has slightly different size R, width l_0 and shape in the plane. The soliton solution represents the structure with the minimal energy for a given number N of spin deviations. Then, for any initial condition used in the simulation, the energy of the system E is larger than the energy of the soliton with given initial moment number N. The initial energy partly transforms into the eigenmodes of the system's continuum spectrum and into the possible internal modes of the soliton itself. To avoid this problem we have applied a damping at the initial stage of simulation. The value of this damping and the time of its acting was fixed in all simulations. However, as the damping of spin waves depends on their frequencies and as the number of excited magnons was different in different cases, we could not damp all these modes exactly in all simulations performed. As we will discuss in the following, some of the simulations still show spin waves at the final step of the procedure.

Another problem is connected to the definition of the final size R of the soliton when the domain wall form slightly differs from the radial symmetrical one and when its shape is different in different azimuthal directions. However, the initial radius R inserted in the simulation does not vary significantly along the procedure and, then, we decided to keep this value as characterizing the soliton size.

We start our simulations by inserting a structure very similar to a soliton at the center of a square lattice of 100×100 spins ($L = 50$). The quasi-2D compounds with Cu magnetic ions have such a square lattice (see Tab. 7 in Ref. [3]). The out-of-plane component of this structure is defined by

$$s_z = \begin{cases} 1: & r < R - l_0' \,, \\ \sin(-\pi(r-R)/l_0): & R - l_0' < r < R + l_0' \,, \\ -1: & R + l_0' < r \,, \end{cases} \tag{34}$$

where R is the soliton radius and the initial shape of soliton is characterised by two parameters: magnetic length $l_0 = 1/\sqrt{4K}$ and the cutoff size l_0' which is taken the same for all simulations: $l_0' = 4$. The parameter l_0' only needs to be larger than one lattice constant so that the initial soliton has a well pronounced vortex in-plane structure. This structure is defined by the function $\phi = \tan^{-1}(y/x)$. The fixed boundary conditions imposing $s_z = 1$ at the border of the lattice are supposed.

We used the discrete equations of motion (6) for unit vectors $\mathbf{s}^n$ in our numerical simulation. In contrast to the analytical calculation described in Sections 3 and 4, we worked here with the Cartesian components s_α. The time integration is done by the same fourth-order Runge-Kutta code as in [33] and [34]. In order to assure precise values for ω, a time integration over 2000 time units is done with an integration step size of 0.01 time units. This choice is good for intermediate K and R values. For example, for $K = 0.1$ with the period of the ferromagnet resonance being $T_0 = 2\pi/\omega_0 \simeq 15.8$ for the soliton radius $R = 20$, it follows from (31) that the period of soliton precession is $T \simeq 200$ and the simulation time contains about 10 oscillations of magnetization in the soliton. However, for smaller values of anisotropy and larger radii, the accuracy on the calculation of the frequency decreases: for $K = 0.01$ and $R = 30, 40$ the total integration time contains only 2 and 1.5 soliton oscillations.

During the first few time steps of integration, the structure adjusts itself to the real conditions of the system by radiating spin waves. The magnons with wave lengths of order of $\lambda \sim 1/R$ and the internal modes localized near circular domain wall are mainly excited. In order to test the soliton stability and, mostly, to damp out the spin waves generated from non ideal initial conditions we have applied a Gilbert damping [35,36] to the first 100 time units of integration ($t < t_0 = 100$). This damping is included in the simulations through the addition of the term $\epsilon\,(\mathbf{s}^n \times \mathrm{d}\mathbf{s}^n/\mathrm{d}t)$ to equation (2) implying that the damping time rate for the spin waves is $\tau \sim 1/\epsilon\omega$. As said

before, we took the same value for ϵ: $\epsilon = 0.02$ in all simulations performed. Then, for spin waves with frequency ω_0, the damping time is $\tau = 25/\sqrt{K}$ and we conclude that for $K < 0.06$ the damping time τ will be larger than t_0 and the spin waves will not damp out completely. Despite these drawbacks, we chose to use small values for ϵ and t_0 in order to avoid the damping of the soliton itself and uncontrolled changing of its size.

We observed that, during the integration process, the soliton radius does not change substantially from the value initially chosen and the final domain wall width l_0 is reached after few time steps suggesting that our initial structure was not too far from the shape of the soliton solution for these systems. This feature contributes to our study of the dependences of the soliton shape on its radius and on its precession frequency.

To find the area of applicability of the analytical approach, of the shooting method, and the boundaries of validity of equation (33), the simulations were done in wide intervals of anisotropy values and soliton radii. The anisotropy constant K was varied in the 0.001 to 40 range and the soliton size R in the interval $1 \leq R \leq 40$. For all these values of (K, R), we obtained the shape of s_z-magnetization component in the soliton (*i.e.*, the profile of magnon density in this magnon droplet) at the final stage of simulation ($t = 2000$), the in-plane magnetization distribution (s_x, s_y) and the density of states of magnetic excitations, particularly the soliton frequencies.

In order to discuss the results, we divide the area of parameters (K, R) into some domains depending on the main features for the soliton structure and dynamics.

(i) When the radius of soliton approaches to the size of the system ($R = 40 \sim L = 50$) the influence of the fixed boundaries can be important. Nevertheless, in a broad anisotropy interval, we soliton observed has circular form in most cases. The boundaring domain wall lost its cylindrical symmetry only in the limits of very small ($K = 0.003$) and large ($K \geq 0.5$) values of anisotropy.

(ii) For strong anisotropy ($K \geq 0.5$), the domain wall transforms into a practically collinear structure. (As we noted in Section 2, the domain wall in a 1D ferromagnet with pure exchange anisotropy never becomes exactly collinear). In this limit, we must use $\cosh(1/l_0^*) = 1 + 2K$ instead of $l_0 = 1/\sqrt{4K}$ for the width of the wall. However, in reality, this width becomes of the order of the interatomic distance for $K \sim 1$. This means that discrete effects are important in this region. For example, the width and energy of the domain wall must depend on its orientation in the lattice and the shape of the wall must deviate from cylindrical one. This effect was predicted in [28]. However, although we have indeed observed non cylindrical solitons for $K = 1$ and $K = 10$, it is important to remark that, in contrast to the predictions in [28], the domain walls tend to orientate along the diagonal of the lattice cell. Nevertheless, as the deviations of the form in most cases were small we can still consider the soliton as having radial symmetry and use the discrete domain wall energy obtained in Section 2 to analyse the dependence of the soliton frequency on its size and anisotropy

$$\omega = \frac{\sqrt{4K}}{R} \frac{\sqrt{1+K}}{1+2K} . \tag{35}$$

This equation corresponds to equation (31) in the discrete limit.

For $K > 40$, the soliton is a stable, static structure resembling a collinear domain wall. Due to this practically collinear structure of soliton there is neither visible in-plane vortex structure nor any spin precession defined. Even for not so large anisotropy values, $K > 0.5$, the width of the domain wall is not large enough to provide a reasonable number of spins with non-zero in-plane components so that the precession frequencies can be measured with sufficient accuracy. But in the intermediate area with $K = 0.5$ we see deviations from equation (31) in the dependence $\omega = \omega(K)$ (see Fig. 2) and this decreasing of frequency is in agreement with (35).

(iii) In the opposite case of small anisotropy, we can consider the vortex as a magnon droplet limited by a domain wall only if the soliton radius is larger then the width l_0 of this wall. In the $R < l_0$ or $K < 1/4R^2$ domain, the topological structure of the vortex center plays an important role and we must use (32) instead of (30) for the soliton profile, and (33) instead of (31) for its frequency. In our simulations in this domain of parameters, the initial vortex structure collapses and solitons break down into spin waves. Note that in this interval of parameters, the initial condition (34) does not correspond to the real magnetization distribution and then the system is highly excited initially. It is probably this circumstance that leads to the solitons collapse. Solitons were observed only for $4KR^2 \sim 10$. The simulations show that for $K = 0.01$ the structure collapses for $R = 10$ ($4KR^2 = 4$) and survives only if $R \geq 20$ ($4KR^2 \geq 16$). However, it is interesting to note that extremely small vortices with $R = 1$ were stable and observed for all values of K from 0.003 to 0.5.

(iv) The domain of parameters $1 < l_0 < R$ is the most interesting because it corresponds to the region where the vortex represents the topological magnon droplet and it becomes possible to compare its structure and dynamics with those obtained from the analytical approach and from the shooting method. However, as the interval of K values where solitons were observed decreases as their size R decreases, we display in the following figures only the results for $10 \leq R \leq 40$ and $0.01 \leq K \leq 0.5$.

We investigated the dependences of the precession frequency ω, the domain wall width l_0 and the number of magnons in the soliton on the anisotropy parameter K and on the soliton radius R. The frequencies were measured from the Fourier spectra of a time evolution of the S_x and S_y spin components from one row of spins. Figure 1 is a logarithmic plot showing the dependence of ω on R for five K values. The curves for $K > 0.01$ look like parallel lines in agreement with the $\omega \sim 1/R$ dependence predicted in (31) and plotted for comparison as a thick line. The curve for $K = 0.01$ is not perfectly parallel to the others and we believe that the cause of this deviation is the lack of precision in the measurement of very low frequencies.

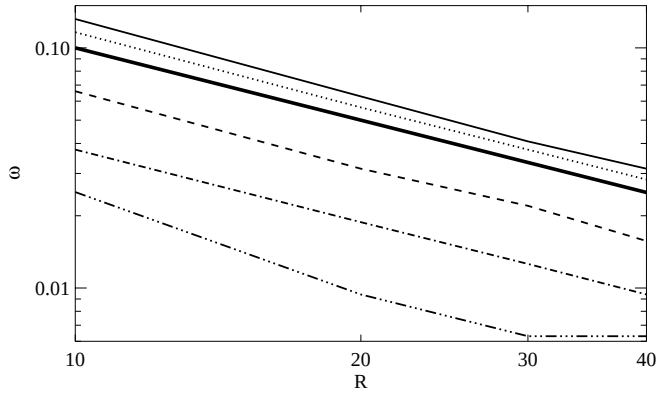

Fig. 1. Precession frequency ω *vs.* soliton radius R. (———) $K = 0.5$; (· · · · · ·) $K = 0.3$; (− − −) $K = 0.1$; (− · − · −) $K = 0.03$; (− · · · −) $K = 0.01$; (▬▬▬) $\omega \sim 1/R$.

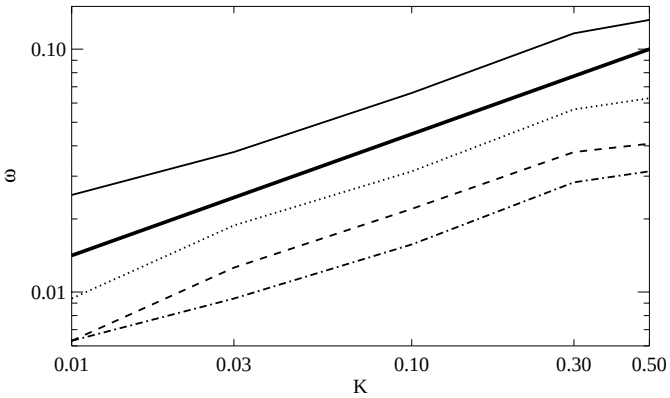

Fig. 2. Precession frequency ω *vs.* anisotropy constant K. (———) $R = 10$; (· · · · · ·) $R = 20$; (− − −) $R = 30$; (− · − · −) $R = 40$; (▬▬▬) $\omega \sim \sqrt{K}$.

For example, $\omega \simeq 0.006$ in the case $K = 0.01$, $R = 40$ and this corresponds to only two rotations of spins during the time of simulation. The dependence of ω (logarithmic scale) on the anisotropy parameter K for several values of the soliton radius is shown in Figure 2. For a large range of K, the curves agree rather well with the relation $\omega \sim \sqrt{K}$ from (31), plotted as a thick line for comparison. In this figure, we note that all frequencies obtained for $K = 0.5$ are smaller than what they should be if the suggested relation (31) between ω and K were valid. However, as we have discussed above, in this region of K the width of the domain wall becomes smaller than a lattice spacing. Then equation (31) transforms into (35) and the frequency must decrease. The deviations in frequency dependence on anisotropy were observed for small K ($K = 0.01$) and large radii R as well. But in this limit we could not evaluate the frequency precisely enough: for $R = 20, 30, 40$ the simulation time $t = 2000$ contained only 6, 4 and 3 periods of spins rotations.

Combining the results obtained in Figures 1 and 2, we conclude that ω is inversely proportional to R and proportional to $\sqrt{K}$. So the dependence $\omega \sim \sqrt{K}/R \sim 1/Rl_0$ similar to the analytical result (31) is valid in all this interval of parameters including the areas of large radii (of the order of the system size) and large anisotropy with the domain wall width being of the order of the interatomic distance.

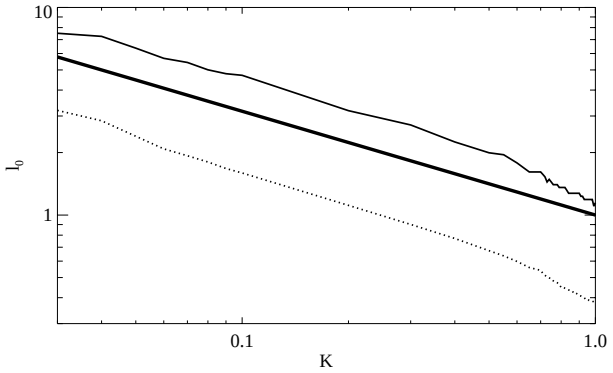

Fig. 3. Domain wall width l_0 *vs.* anisotropy constant K. $R = 15$. (———) Counting method; (· · · · · ·) Fitting method; (▬▬▬) $l_0 = 1/\sqrt{K}$.

The domain wall widths l_0 were determined by two methods. First, we fitted $\theta(r)$ to a function very similar to equation (30)

$$\theta_{\rm f}(r) = \pi - 2\arctan\exp\left(\frac{r - R_{\rm f}}{l_{\rm f}}\right) \qquad (36)$$

where $R_{\rm f}$ and $L_{\rm f}$ are the fitting parameters. We found that (36) is very close to the real soliton shape. We also determined l_0 by simply counting those spins which are not completely aligned along the z-axis (*i.e.*, we considered all spins with $-0.9 < S_z < 0.9$ and divided the obtained number by $2\pi R$). These two estimates for l_0 are plotted as a function of K in Figure 3: both results give curves very close to straight lines although there is a non-negligible deviation for large anisotropies ($K \geq 0.5$), when the width is governed by the discreteness of the system and is different in different points along the domain wall. We conclude then that the dependence of the domain wall width on K is $l_0 \sim 1/\sqrt{K}$, as predicted by our analytical approach and by the numerical solution of (22).

At last, we measured the magnon number N of the simulated solitons applying formulae (14) to the obtained in simulation spin fields. The result is shown in Figure 4 where we can see that the relation $N = 2\pi R^2$ is very well fulfilled although there are slight deviations for small K and small R. These deviations are caused by the large wall width l_0. It is easy to show that for the symmetric domain wall profile in a fitting function like (36), the total number of magnons in a soliton is $N = 2\pi R^2 - \mathcal{O}(Rl)$ (or $\ln N \sim 2\ln R - \mathcal{O}(1/R\sqrt{K})$) and small deviations from the parabolic law increase with the decreasing of $R\sqrt{K}$.

Finally, we compare the shape of the soliton obtained from the numerical solution of (22) to the soliton shape obtained from the spin dynamic simulation. Therefore, we insert the frequencies ω measured from the simulations

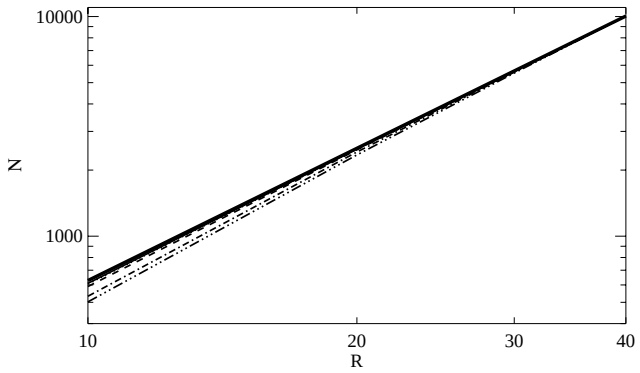

Fig. 4. Magnon number N *vs.* soliton radius R. (———) $K = 0.5$; (· · · · · ·) $K = 0.3$; (− − −) $K = 0.1$; (− · − · −) $K = 0.03$; (− · · · −) $K = 0.01$; (———) $N = 2\pi R^2$.

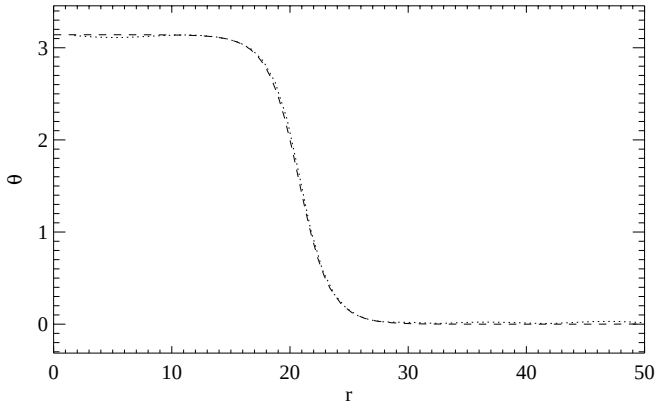

Fig. 5. Numerical solution of (22) for $R_0 = 20$, $K = 0.1$, and $\omega = 0.0314$ (dashed line), compared to the shape of the soliton obtained in the spin dynamics simulations (dotted line).

into the differential equation (22) and implement the numerical solution of this equation as explained before. The two results for $K = 0.1$, $R = 20$, and $\omega = 0.0314$ are shown in Figure 5 where it can be seen that the agreement is very good: both the shape of the wall and its width are in excellent agreement in the two calculations. The domain wall radius R_0 does not change appreciably for $0 < K < 0.1$. For $K = 0.5$ the radius determined by the numerical solution is larger (by up to four lattice units) than the one obtained by the simulations. However, we have already seen that for anisotropies of this magnitude (and higher) the discreteness of the system becomes important and we cannot expect a good agreement between the two different calculations. We also obtain a discrepancy in the comparison of the two soliton shapes for very small anisotropy, $K = 0.01$, where the continuous approach must be valid. The problem here seems to be the precision in the measurement of small frequencies, as mentioned before.

6 Conclusion

In the article we provide a complex analysis of the structure and dynamics of topological solitons in ferromagnets with exchange easy-axis anisotropy both numerically and analytically. The numerical simulations have been done in wide intervals for the anisotropy parameter K and for the soliton size R. The dependencies of the soliton shape, the frequency ω of spin rotations in the soliton, the width l_0 of the domain wall bordering it, and the number N of magnons bound in the soliton on the parameters K and R were found. We obtained the following main results:

(i) In wide intervals of exchange anisotropy and of the soliton size, the topological soliton represents the magnon droplet bounded by a domain wall and is practically similar to solitons in ferromagnets with pure single-ion anisotropy.

(ii) In this domain of the parameters, all structural and dynamical characteristics of the soliton obtained from numerical simulations (with good accuracy) coincide with the results of our analytical approach and with the data of numerical calculation performed with the shooting method.

(iii) The numerical simulations show that in the intermediate areas with $l_0 \sim a$ and $l_0 \sim R$, the analytical predictions for $\omega = \omega(K, R)$, $l_0 = l_0(K)$ and $N = N(K, R)$ can be considered to hold qualitatively.

(iv) In the limit of strong anisotropy ($K > 0.5$), the soliton transforms into a nearly collinear localized structure with non evident topological properties. In this limit, solitons with large radii can loose their radial symmetry due to the discreteness of the lattice and influences from the boundaries.

(v) In the opposite case $l_0 > R$, the magnon droplet transforms into a soliton with evident topological structure. But our numerical simulations demonstrate that, in this limit, solitons become less stable and brake down into spin waves from excited initial states.

We must stress that the last results (iii, iv, v) were obtained by numerical simulations performed in domains of parameters where another methods of investigation of solitons are non applicable.

In the Introduction, we stressed that according to a simple theoretical approach, magnetic vortices exist rather in 2D ferromagnets than in 2D antiferromagnets. Consequently, all calculations in this paper were realized for easy-axis ferromagnets. It will be interesting to provide experiments similar to those performed in [7] but for quasi-2D ferromagnets. There exists a large variety of such compounds (see Tab. 7 from [3]) with a wide interval of magnetic anisotropy values ($K \sim 10^{-2} \div 10^{-5}$). However, as the magnetic vortex is the dynamical object, it is important to investigate experimentally the density of states in the frequency gap $\omega < \omega_0$. In Section 6 (see (iii)), we showed that, according to our simulations, the minimum size of observed vortices with minimum energies was $R \sim l_0$. The corresponding ratio ω/ω_0 varied in the interval (0.2−0.5) in the depth of the gap. So we may hope that such frequencies may be detected experimentally.

The authors gratefully acknowledge the support of CAPES-DAAD (project PROBRAL).

References

1. A.M. Kosevich, B.A. Ivanov, A.S. Kovalev, Phys. Rep. **194**, 117 (1990).
2. V.G. Bar'yakhtar, B.A. Ivanov, Sov. Sci. Rev. A **16**, 1 (1992).
3. L.J. de Jong, A.R. Miedema, Adv. Phys. **23**, 2 (1974).
4. A.A. Anders, V.G. Borisenko, S.V. Volotskii, Sov. J. Low Temp. Phys. **15**, 21 (1989).
5. H.R. Boesch, U. Schmocker, F. Waldner, K. Emerson, J.E. Dramheller, Phys. Lett. **36**, 461 (1971).
6. H. Hagen, H. Reimann, U. Schmocker, F. Waldner, Physica B **36–38**, 461 (1971).
7. F. Waldner, J. Magn. Mag. Matter **31–34**, 1203 (1983).
8. F. Waldner, J. Magn. Mag. Matter **54–57**, 837 (1986).
9. A.A. Stepanov, M.I. Kobets, V.A. Pashchenko, Low Temp. Phys. **20**, 221 (1994).
10. H. Yamazaki, M. Mino, Progr. Theor. Phys. Suppl. **94**, 400 (1989).
11. A.I. Zvyagin, V.N. Krivoruchko, V.A. Pashchenko, Sov. Phys. JETP **65**, 177 (1987).
12. A.M. Pshisukha, A.I. Zvyagin, A.A. Stepanov, Sov. Phys. Solid. State **13**, 2630 (1971).
13. M.V. Gvozdikova, A.S. Kovalev, Yu. S.Kivshar, Low Temp. Phys. **24**, 479 (1998).
14. M.V. Gvozdikova, A.S. Kovalev, Low Temp. Phys. **24**, 808 (1998).
15. A.S. Kovalev, M.V. Gvozdikova, Low Temp. Phys. **25**, 184 (1999).
16. A.S. Kovalev, A.M. Kosevich, K.V. Maslov, JETP Letters **30**, 296 (1979).
17. A.M. Kosevich, B.A. Ivanov, A.S. Kovalev, Physica D **3**, 363 (1981).
18. A.M. Kosevich, V.P. Voronov, Sov. J. Low Temp. Phys. **7**, 442 (1990).
19. M.E. Gouvea, G.M. Wysin, A.R. Bishop, F.G. Mertens, Phys. Rev. B **39**, 11840 (1989).
20. F.G. Mertens, A.R. Bishop, *Dynamics of vortices in two-dimensional magnets*, in *Nonlinear Science at the dawn of the 21st Century*, Lecture Notes in Physics, edited by P.L. Christiansen, M.P. Sœrensen, A.C. Scott (Springer, Berlin, 2000).
21. F. Waldner, Phys. Rev. Lett. **65**, 1519 (1990).
22. A.S. Kovalev, Ph.D. thesis, University of Kharkov, 1989.
23. B.A. Ivanov, B.A. Stephanovich, JETP **91**, 638 (1986).
24. B.A. Ivanov, B.A. Stephanovich, A.A. Zhmudskii, J. Magn. Mag. Matter **88**, 116 (1990).
25. A.S. Kovalev (unpublished).
26. J.J. Van der Broek, H. Zijlstra, IEEE Trans. Magn. V. Mag. **7**, 226 (1971).
27. A.N. Goncharuk, A.A. Stepanov, D.A. Yablonskii, Sov. J. Solid State **31**, 2099 (1989).
28. I.G. Gochev, Sov. Phys. JETP **58**, 115 (1983).
29. A.M. Kosevich, B.A. Ivanov, A.S. Kovalev, *Nonlinear magnetization waves. Dynamical and topological solitons* (in Russian) (Naukova Dumka, Kiev, 1988).
30. A.M. Kosevich, B.A. Ivanov, A.S. Kovalev, Sov. Sci. Rev. A **6**, 161 (1985).
31. N. Papanicolaou, T.N. Tomaras, Nucl. Phys. B **360**, 425 (1991).
32. N. Papanicolaou, W.J. Zakrzewski, Physica D **80**, 225 (1995).
33. W.H. Press, S.A. Teukolsky, W.T. Vetterling, B.P. Flannery, *Numerical Recipes in FORTRAN* (Cambridge University Press, 1992).
34. F.G. Mertens, H.-J. Schnitzer, A.R. Bishop, Phys. Rev. B **56**, 2510 (1997).
35. T. Kamppeter, F.G. Mertens, A. Sánchez, A.R. Bishop, F. Domínguez-Adame, N. Grønbech-Jensen, Eur. Phys. J. B **7**, 607 (1998).
36. S. Iida, J. Phys. Chem. Solids **24**, 625 (1963).